Check for updates

Received: 3 January 2022 | Revised: 18 June 2022 | Accepted: 27 June 2022

DOI: 10.1002/pip.3607

RESEARCH ARTICLE

PROGRESS IN PHOTOVOLTAICS WILEY

# Tube-type plasma-enhanced atomic layer deposition of aluminum oxide: Enabling record lab performance for the industry with demonstrated cell efficiencies >24%

Baochen Liao[1,2] | Xinyuan Wu[2,3] | Weiliang Wu[4] | Changming Liu[5] | Sheng Ma[2,6] | Shaozhou Wang[3] | Tong Xie[3] | Qiang Wang[1] | Zheren Du[7] | Wenzhong Shen[6] | Xiang Li[2] | Weimin Li[2] | Bram Hoex[3]

[1]School of Information Science and Technology, Nantong University, Nantong, Jiangsu, China

[2]Jiangsu Leadmicro Nano-Equipment Technology Ltd., Wuxi, Jiangsu, China

[3]School of Photovoltaic and Renewable Energy Engineering, University of New South Wales, Sydney, Australia

[4]Tongwei Solar Co., Ltd., Meishan, Sichuan, China

[5]Jinko Solar Holding Co., Ltd., Haining, Zhejiang, China

[6]Institute of Solar Energy, Shanghai Jiao Tong University, Shanghai, China

[7]Jolywood Solar Technology Co. Ltd., Taizhou, Jiangsu, China

**Correspondence**
Baochen Liao, School of Information Science and Technology, Nantong University, Nantong, Jiangsu 226019, China.
Email: liaobaochen@ntu.edu.cn

Xinyuan Wu and Weimin Li, Jiangsu Leadmicro Nano-Equipment Technology Ltd., Wuxi, Jiangsu 214028, China.
Email: xinyuan.wu@unsw.edu.au; weiming.li@leadmicro.com

Weiliang Wu, Tongwei Solar Co., Ltd., Meishan, Sichuan 620010, China.
Email: wuwl02@tongwei.com

**Funding information**
Major State Basic Research Development Program of China, Grant/Award Number: 2018YFB1500501; Construction Fund for School of Tongke Microelectronics, Nantong University, Grant/Award Number: 0702610104; Major Program for the Natural Science Research of the Higher Education Institutions of Jiangsu Province, China, Grant/Award Number: 19KJ320004; Research Funding for High-level Talents of Nantong University, Grant/Award Number: 03083035; Jolywood Solar Technology Co. Ltd; Tongwei Solar Co., Ltd.; Jinko Solar Holding Co., Ltd.; Leadmicro Nano-Equipment Technology Ltd.

## Abstract

In this work, single-side aluminum oxide ($Al_2O_3$) deposition enabled by a new tube-type industrial plasma-assisted atomic layer deposition (PEALD) technique is presented to meet the increasingly stringent requirements for high-efficiency solar cell mass production. Extremely low emitter saturation current densities, $J_{0e}$, down to 15 fA/cm$^2$ are achieved on an industrial textured boron emitter with a sheet resistance of 104 Ω/sq, passivated by PEALD $Al_2O_3$/PECVD $SiN_x$ stack after firing. An implied open-circuit voltage of up to 721 mV is obtained on symmetrical lifetime samples. The underlying passivation mechanisms of this new tube-type PEALD $Al_2O_3$ are investigated by contactless corona-voltage measurements. The results indicate that the superior passivation is mainly attributed to a low interface defect density down to $1.1 \times 10^{11}$ cm$^{-2}$ eV$^{-1}$ and a high negative fixed charge density up to $4.5 \times 10^{12}$ cm$^{-2}$. Simulations show that the obtained $J_{0e}$ is close to its intrinsic limit. Lastly, the developed tube-type PEALD $Al_2O_3$ is applied to industrial TOPCon solar cells achieving an average cell efficiency above 24% and a maximum $V_{oc}$ of 707 mV. This work shows that the record level of surface passivation available from lab-scale PEALD reactors is now available in a flexible high-throughput industrial PEALD platform, which opens a new route for mass production of high-efficiency industrial TOPCon solar cells with a lean process at low costs.

**KEYWORDS**
aluminum oxide, boron emitter passivation, industrial tube PEALD, interface oxide, TOPCon

 © 2022 John Wiley & Sons Ltd. 

## 1 | INTRODUCTION

The current mainstream industrial crystalline silicon (*c*-Si) solar cell is based on the passivated emitter and rear cell (PERC) technology, which was first introduced in the late 1980s with an efficiency of 22.8%[1] and achieved a record efficiency of 25% with the passivated emitter and rear local contact (PERL) structure in the late 1990s.[2] In recent years, the PERC cells have been well developed, with a mass production average cell efficiency of ~23% in 2021 and a champion efficiency of 23.83% for a commercial *p*-type Czochralski (Cz) PERC cell reported by Longi solar in the 2020s.[3] However, this cell performance is approaching its practical limit.[2,4–8] The efficiency of the industrial PERC cell is limited by the recombination losses at the metal contacts and recombination in the *c*-Si bulk.[9] Passivating contacts have been proposed to reduce the losses due to the metal contacts for the next-generation industrial high-efficiency silicon solar cells.[5,10–12] The best-known example of a solar cell with passivating contacts for both electrons and holes is the heterojunction with intrinsic thin layer (HIT) solar cell[13–20] with a record efficiency of 25.54%[21] for a bifacial solar cell and 26.7%[19] in an interdigitated back contact (IBC) design. Another good example is the tunnel oxide passivated contact (TOPCon) solar cell,[10,22–31] which features a passivating electron contact with a record efficiency of 25.8%[25] on *n*-type *c*-Si, 26.0%[32] on *p*-type *c*-Si, and 26.1%[33] for an IBC solar cell. Unlike the HIT solar cell, the TOPCon solar cell fabrication process is compatible with the well-developed PERC solar cell fabrication technology, making it the ideal candidate for upgrading existing PERC lines.

Instead of the *p*-type wafers used for the vast majority of PERC cells, *n*-type *c*-Si wafers are commonly used for industrial TOPCon solar cells. They have a higher bulk lifetime, are less sensitive to most metal impurities, and do not suffer from boron-oxygen related degradation.[34–36] In addition, excellent surface passivation with a surface saturation current density ($J_0$) lower than 5 fA/cm$^2$[28,37] can be achieved for the passivating electron contact at the rear of a TOPCon solar cell. The TOPCon solar cell efficiency is currently limited by recombination at the front boron-doped surface,[25,32] which also has a larger surface area due to the pyramid textured front of the solar cell. Negatively charged aluminum oxide ($Al_2O_3$) is the ideal candidate to passivate the *p*-type boron emitter surface.[38–42] To date, the photovoltaic industry is predominantly using plasma-enhanced chemical vapor deposition (PECVD) or thermal atomic layer deposition (ALD) for the deposition of the $Al_2O_3$ films. Unfortunately, the level of surface passivation on highly doped *p*-type *c*-Si provided by industrial PECVD and thermal ALD $Al_2O_3$ is limiting the performance of TOPCon solar cells due to its high sensitivity of recombination at the front surface. The best results in the lab on highly doped *p*-type *c*-Si have been obtained by plasma-enhanced atomic layer deposited (PEALD) $Al_2O_3$ due to its relatively high fixed charge density ($Q_f$) compared with $Al_2O_3$ films grown by other deposition techniques.[43] PEALD shares all the intrinsic advantages of ALD technology, such as precise thickness control, excellent uniformity, and conformity over large areas, making it an ideal deposition method for any textured surface.[44,45] However, the main drawback of the ALD method for solar cell manufacturing is the difficulty of avoiding wrap-around deposition, which can result in challenges in the rear metallization and rear optics.

In this work, we will present a novel industrial low-cost high-throughput single-side tube-based PEALD $Al_2O_3$ process. This PEALD process can be integrated into tube-PECVD systems commonly used in the manufacturing of PERC cells and are popular for its low cost of ownership (COO) due to lower equipment cost, smaller footprint, higher uptime, and low maintenance cost. These tube-type PEALD/PECVD would feature different tubes for different deposition technology and would significantly simplify the manufacturing complexity and reduce the cost compared with the current standalone thermal ALD $Al_2O_3$ system plus the tube-type PECVD $SiN_x$ system for TOPCon application. Extremely low $J_{0e}$ values down to 14.6 fA/cm$^2$ and $iV_{oc}$ up to 721 mV were achieved on an industrial textured boron emitter with a sheet resistance of 104 Ω/sq. The underlying passivation mechanism of the tube-type PEALD $Al_2O_3$ was investigated by contactless corona-voltage measurements. The results indicated that the superior passivation was mainly attributed to a low interface defect density $D_{it}$ (down to 1.1 × 10$^{11}$ cm$^{-2}$ eV$^{-1}$) and a high fixed charge density $Q_f$ (up to −4.5 × 10$^{12}$ cm$^{-2}$). Simulation shows that the obtained $J_{0e}$ values were very close to their intrinsic limit value, where $J_{0e}$ is solely ruled by Auger recombination in the boron emitter. Lastly, the developed tube-type PEALD $Al_2O_3$ was applied to industrial TOPCon solar cells, and an average cell efficiency above 24% with a maximum $V_{oc}$ of 707 mV was obtained. This work shows that record lab-scale performance is now available in a high-throughput industrial tool, making tube-type PEALD $Al_2O_3$ a strong candidate for boron emitter passivation for TOPCon solar cells.

## 2 | EXPERIMENTAL DETAILS

To investigate the level of surface passivation, symmetrical lifetime samples were prepared based on the process flow shown in Figure 1. G12-sized (170 μm, 441 cm$^2$) Czochralski (Cz) *n*-type silicon wafers with a resistivity of 0.3 to 2.1 Ω·cm were used. The wafers were firstly saw damage etched (SDE) in potassium hydroxide (KOH) followed by an alkaline texturing on both sides of the wafer, resulting in a pyramid size of ~2 μm. After cleaning, boron diffusion was performed in a tube furnace using boron trichloride ($BCl_3$) as dopant source, thus resulting in a symmetrical $p^+np^+$ structure with an emitter sheet resistance of ~104 Ω/sq. Subsequently, the borosilicate glass (BSG) layer was stripped in a diluted (10%) hydrofluoric acid (HF) solution until the surface became hydrophobic. After cleaning, a ~3 nm $Al_2O_3$ film was deposited on both sides of the samples using a tube-type PEALD system (ZR5000, LeadMicro, 480 pcs/tube for 210 mm wafers, 6 tubes/system, throughput ~9000 pcs/h). For the PEALD $Al_2O_3$ process, trimethylaluminum (TMA) [Al $(CH_3)_3$] (solar grade 5N, Nata Opto-electronic Material) was used as the aluminum precursor, and an $O_2$ plasma was used as the oxidant, generated by a direct radio frequency (RF) plasma source operating at 40 kHz and a power of 12 kW. The growth-per-cycle (GPC) was ~1.14 Å/cycle, the pulse

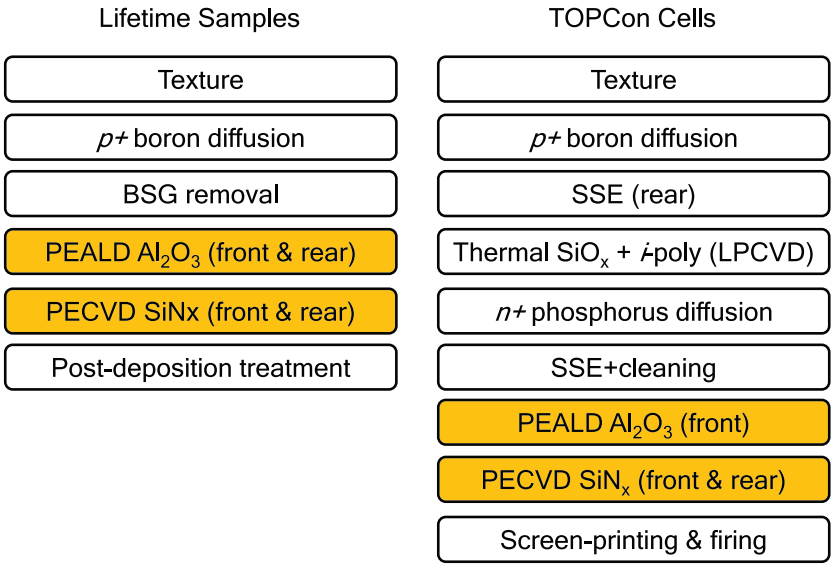


**FIGURE 1** The fabrication process flows for the lifetime samples and the bifacial TOPCon silicon solar cells [Colour figure can be viewed at wileyonlinelibrary.com]

time for both TMA and $O_2$ plasma was about 4 s, and the cycle time was ~25 s; 30 ALD cycles were used to achieve a 3-nm $Al_2O_3$ film. All films were deposited at a substrate temperature of 200°C. Subsequently, a ~70 nm $SiN_x$ film was deposited on both sides of the samples in a different tube of the same PECVD reactor. After that, the symmetrical samples underwent a rapid thermal anneal in an industrial fast firing furnace for a few seconds (set peak temperature 800°C), followed by an industrial light-induced annealing furnace (light soaking) for a few seconds.

To verify the performance of the developed industrial tube-type PEALD $Al_2O_3$ passivation at the device level, industrial TOPCon cells were fabricated based on the process flow shown in Figure 1, and the resulting cell structure is shown in Figure 2. After SDE and texturing on both sides, boron diffusion was carried out to form a $p^+$ layer. Subsequently, an inline single-side etch (SSE) was performed to remove the $p^+$ doping and polish the rear surface. After cleaning, an interfacial thermal oxide and an intrinsic polysilicon (*i*-poly) layer were deposited at the rear surface by an industrial low-pressure chemical vapor deposition (LPCVD) tool. Phosphorus diffusion was carried out to dope the *i*-poly layer and form the $n^+$ polysilicon layer. Subsequently, an inline single-side etch (SSE) was performed to remove the wrap-around $n^+$ layer at the front surface. After cleaning, the front $p^+$ surface was passivated by a thin film stack consisting of ~3-nm PEALD $Al_2O_3$ film and ~70-nm PECVD $SiN_x$ film, while the rear surface was coated with a ~70-nm $SiN_x$ film. All thin films were deposited by an industrial tube-type PEALD/PECVD system (ZR5000, LeadMicro). Lastly, the samples were screen-printed on both sides with an Al-Ag alloy paste for the front and Ag paste for the rear (both with 12 busbars). The cells were then fired at a peak temperature of around 800°C (set temperature was used, unless stated otherwise) using an industrial fast-firing furnace, followed by an illuminated anneal in an industrial furnace for a few seconds.

The passivation quality of the $Al_2O_3$ film was quantified by measuring the effective minority charge carrier lifetime of the symmetrically passivated $p^+np^+$ structures using a contactless

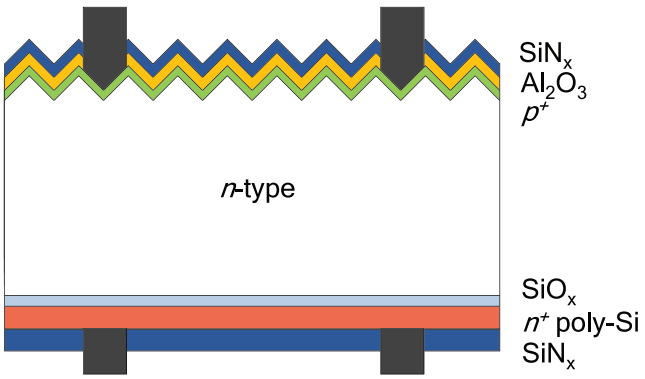


**FIGURE 2** Schematic of a tube-type PEALD $Al_2O_3$ passivated *n*-type bifacial TOPCon silicon solar cell [Colour figure can be viewed at wileyonlinelibrary.com]

photoconductance decay (PCD) tester (WCT-120, Sinton Instruments). The implied open-circuit voltage ($iV_{oc}$) of the samples was extracted according to the method published by Sinton and Cuevas.[46] The emitter saturation current density ($J_{0e}$) was determined according to the high-injection method proposed by Kane and Swanson[47]:

$$\frac{1}{\tau_{eff}} - \frac{1}{\tau_{Auger}} = \frac{1}{\tau_{SRH}} + \frac{2J_{oe}(N_d + \Delta n)}{qn_i^2 W} \quad (1)$$

where $\tau_{eff}$ is the measured effective carrier lifetime of the sample, $\tau_{Auger}$ the intrinsic Auger lifetime,[48] $\tau_{SRH}$ the defect-related Shockley-Read-Hall bulk lifetime, $N_d$ the bulk doping concentration, $\Delta n$ the excess carrier density, $q$ the elementary charge, $n_i$ the intrinsic carrier concentration, and $W$ the sample thickness. The presented $J_{0e}$ values were evaluated at 25°C, with a corresponding $n_i$ of $8.6 \times 10^9$ $cm^{-3}$.[49,50] The measurements of $J_{0e}$ to be accurate within 3% to 7%.[51] The emitter sheet resistance was determined by a four-point probe measurement. The active dopant depth profile was

measured by electrochemical capacitance-voltage (ECV) profiling (WEP, CVP21). The surface passivation mechanism and the interface properties were studied by using contactless corona-voltage (*C-V*) measurements (PV2000, Semilab). Undiffused *n*-type planar samples with 10-nm PEALD $Al_2O_3$ films on both sides were used. These measurements are not feasible on highly doped samples as the applied corona charge will be screened by the highly conductive diffused layer so that a transition from accumulation to inversion (which is needed for $Q_f$ and $D_{it}$ evaluation) can no longer take place. The procedure of determination of the fixed charge density ($Q_f$) and the energy-level dependent interface defect density $D_{it}$ ($E$) from the contactless *C-V* measurements is discussed in detail elsewhere.[52–54] The ECV and contactless *C-V* results were used to model the theoretical $J_{0e}$ using EDNA 2 from PV Lighthouse.[55] The commonly used physical models to describe silicon wafer-based solar cells such as carrier mobility model by Klaassen,[56,57] intrinsic bandgap by Passler,[58] the density of states from Sentaurus, dopant ionization by Altermatt,[59] Fermi-Dirac statistics,[60,61] bandgap narrowing by Schenk,[62] and the effective intrinsic carrier density by Altermatt,[63] were used in the simulations. The radiative recombination was modeled using the model proposed by Trupke et al.[64] As the emitter region was heavily doped, we assumed no Shockley-Read-Hall (SRH) recombination in the emitter, and the calculation of the surface SRH was done according to McIntosh et al.[65] The empirical Auger parameterization model by Richter[66] was used to model Auger recombination in the emitter and bulk. Full-area current–voltage (*I-V*) measurements were conducted using a *Halm* inline measurement system (cetisPV-IUCT-3600-BF) calibrated using a reference cell from Fujian Metrology Institute, National PV Industry Measurement and Testing Center.

## 3 | RESULTS AND DISCUSSION

### 3.1 | Experimental results on symmetrically passivated textured boron emitters

The boron emitter dopant profile was measured by ECV and the result is shown in Figure 3. The emitter had a surface doping concentration of $\sim 7.4 \times 10^{18}$ cm$^{-3}$ and a junction depth of $\sim$1.1 μm. The sheet resistance of the emitter was $\sim$104 Ω/sq as determined by a four-point probe measurement. The measured Auger-corrected inverse effective minority carrier lifetime for light-soaked $p^+/n/p^+$ samples, symmetrically passivated by 3-nm $Al_2O_3$ and 70-nm $SiN_x$ stack is shown in Figure 4. A linear relation between the Auger-corrected inversion lifetime and the injection carrier density was obtained from moderate to high injection levels [(0.5–2.0) $\times 10^{16}$ cm$^{-3}$]. Hence, $J_{0e}$ could be extracted from the slope of the linear function according to Equation (1). In this work, $J_{0e}$ was extracted at an injection level of $1 \times 10^{16}$ cm$^{-3}$, and the corresponding $J_{0e}$ values were in the range of 15 to 19 fA/cm$^2$.

The measured effective lifetime and the corresponding $iV_{oc}$ for the symmetrically passivated textured $p^+/n/p^+$ samples after firing and light soaking treatment are shown in Figure 5. An average

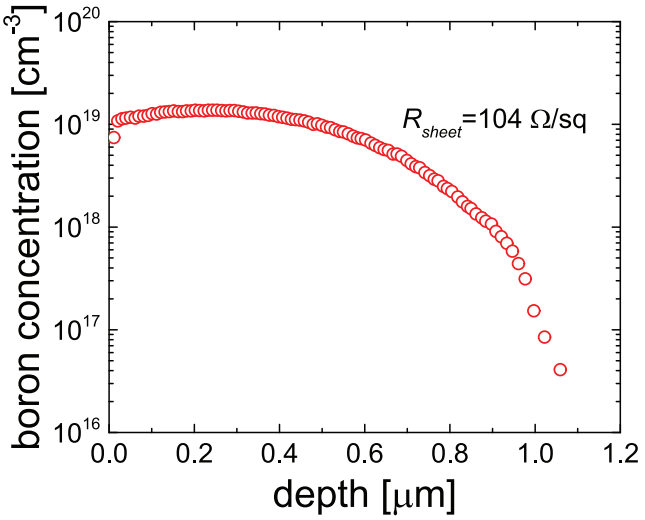


**FIGURE 3** Active boron depth profile of the $p^+$ emitter as determined by ECV. The sheet resistance determined by four-point probe measurement is also shown. [Colour figure can be viewed at wileyonlinelibrary.com]

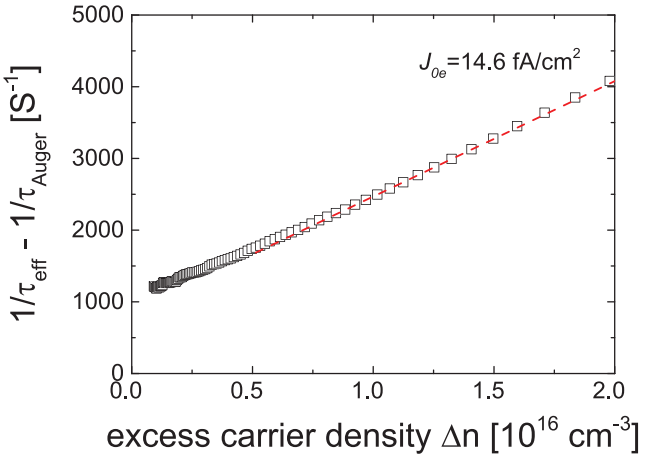


**FIGURE 4** Measured Auger corrected inverse effective minority charge carrier lifetime as a function of the injection level for symmetrical textured $p^+/n/p^+$ samples symmetrically passivated by 3-nm $Al_2O_3$/70-nm $SiN_x$ stack after firing and light soaking treatment. The solid line is a linear $J_{0e}$ that fits the measured data. [Colour figure can be viewed at wileyonlinelibrary.com]

effective lifetime value of 816 μs with corresponding $iV_{oc}$ up to 721 mV was achieved. The state-of-the-art $J_{0e}$ values reported for other deposition methods on textured boron emitters are shown in Figure 6 and compared with the results obtained in this work. Only results on textured samples are shown to ensure an apples-to-apples comparison. It should be noted that the Auger- and defect-related recombination in the various boron emitters used in the various studies could be significantly different due to differences in the process conditions used. As can be seen, excellent boron emitter passivation

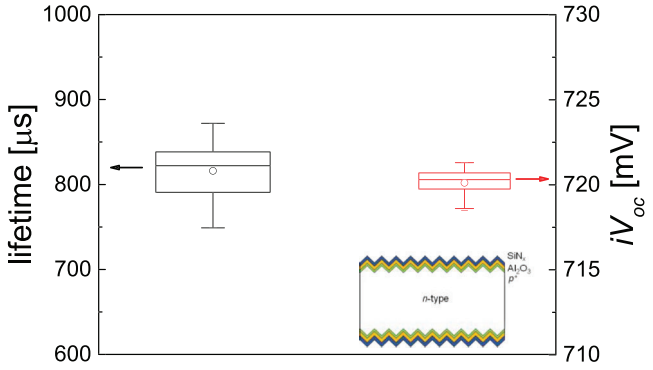


**FIGURE 5** Measured lifetime values (left axis) and corresponding implied $V_{oc}$ values (right axis) of symmetrical textured boron emitter samples after firing and light soaking treatment. Eight samples were prepared and five points (center and four corners) were measured on each sample. Boxes, 25–75% range; vertical lines, maximum and minimum; horizontal lines within boxes, median; circle shape within boxes, mean [Colour figure can be viewed at wileyonlinelibrary.com]

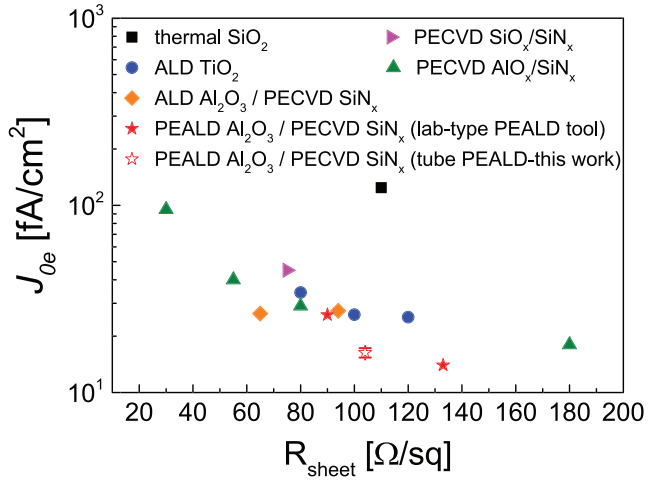


**FIGURE 6** Measured emitter saturation current density $J_{0e}$ as a function of boron emitter sheet resistance passivated by an industrial tube-type system PEALD $Al_2O_3$/PECVD $SiN_x$ stack (this work), compared with textured boron emitters passivated by thermal $SiO_2$,[67] ALD $TiO_2$,[68] ALD $Al_2O_3$/PECVD $SiN_x$ stack,[69] PEALD $Al_2O_3$/PECVD $SiN_x$ stack (lab-type PEALD tool),[72,73] PECVD $AlO_x$/$SiN_x$ stack,[70] and PECVD $SiO_x$/$SiN_x$ stack.[71] The error bars correspond to the standard deviation of 40 data points (eight samples and five points/sample) measured. [Colour figure can be viewed at wileyonlinelibrary.com]

has been achieved in this work by industrial tube-type PEALD $Al_2O_3$ and PECVD $SiN_x$ stack. The $J_{0e}$ values obtained in this work are at least a factor of two lower compared with results reported for textured boron emitters passivated by thermal $SiO_2$,[67] ALD $TiO_2$,[68] ALD $Al_2O_3$/PECVD $SiN_x$ stack,[69] PECVD $AlO_x$/$SiN_x$ stack,[70] and PECVD $SiO_x$/$SiN_x$ stack.[71] This result is comparable with the lab-type PEALD $Al_2O_3$/PECVD $SiN_x$ stack,[72,73] demonstrating that the industrial-scale PEALD tool can provide the same high-quality layers as obtained in the literature by the lab-type PEALD tools.

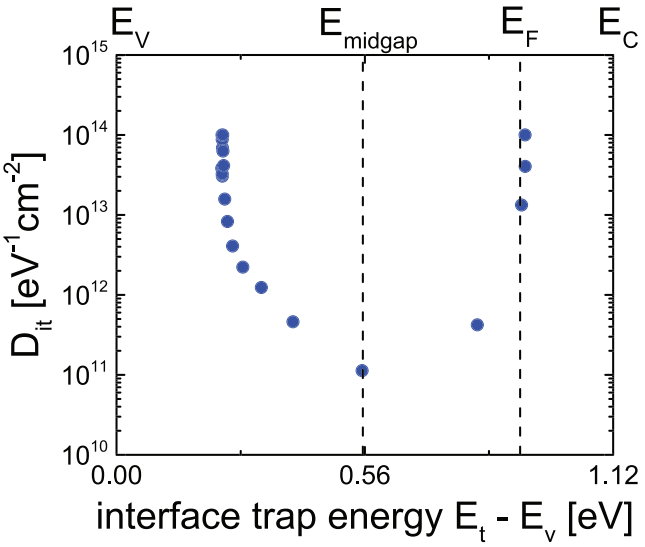


**FIGURE 7** Measured interface defect density $D_{it}(E)$ at the $c$-Si/$Al_2O_3$ interface as a function of interface trap energy ($E_t$) with respect to silicon's valence band energy ($E_v$) for the $Al_2O_3$ (10 nm) passivated undiffused $n$-type $c$-Si sample after firing and light soaking [Colour figure can be viewed at wileyonlinelibrary.com]

### 3.2 | Electronic properties of the c-Si/PEALD $Al_2O_3$ interface

To understand the surface passivation mechanism of the developed tube-type PEALD $Al_2O_3$ film in more detail, contactless corona-voltage measurements were carried out on undiffused silicon samples after firing and light soaking. The measured interface defect density $D_{it}(E)$ at the $c$-Si/$Al_2O_3$ interface as a function of interface trap energy ($E_t$) with respect to silicon's valence band energy ($E_v$) for the $Al_2O_3$ (10 nm) passivated un-diffused $n$-type $c$-Si sample after firing and light soaking is shown in Figure 7. A $D_{it}$ at midgap of $1.1 \times 10^{11}$ $cm^{-2}$ $eV^{-1}$ and an average $Q_f$ of $-4.4 \times 10^{12}$ $q/cm^2$ were obtained, indicating an excellent chemical passivation and field-effect passivation by the tube-type PEALD $Al_2O_3$ process. For comparison, a summary of typical $D_{it}$ and $Q_f$ values reported in the literature for $Al_2O_3$ films grown by various ALD methods is listed in Table 1. As can be seen from Table 1, the $D_{it}$ and $Q_f$ values obtained from the developed industrial tube-type PEALD $Al_2O_3$ in this work are comparable with the state-of-the-art laboratory results by the remote plasma PEALD technology. Table 1 also clearly illustrates that PEALD can achieve significantly higher negative fixed charge densities than thermal or $O_3$ ALD. As field-effect passivation scales with the square of the fixed charge density, this improves surface passivation of a factor of 3.4 compared with thermal ALD and 1.7 compared with $O_3$-ALD.

### 3.3 | Simulated $J_{0e}$

Using the experimentally determined electronic interface parameters and the measured dopant profile, we quantified the $J_{0e}$ using EDNA

**TABLE 1** A comparison of $D_{it}$ and $Q_f$ for $Al_2O_3$ under different anneal conditions and deposition methods

| Deposition method | Anneal condition | $Q_f$ (q/cm$^2$) | $D_{it}$ (cm$^{-2}$ eV$^{-1}$) | Ref. |
|---|---|---|---|---|
| PEALD (remote-plasma) | Annealed (400°C), $N_2$, 10 min | $-5.8 \times 10^{12}$ | $1 \times 10^{11}$ | Dingemans et al.[43] |
| $O_3$-ALD | | $-3.4 \times 10^{12}$ | $1 \times 10^{11}$ | |
| $H_2O$-ALD | | $-2.4 \times 10^{12}$ | $1 \times 10^{11}$ | |
| Industrial tube-type PEALD (direct-plasma) | Fired (800°C) + light-soaked, air, 30s | $-4.5 \times 10^{12}$ | $1.1 \times 10^{11}$ | This work |
| | | $-4.3 \times 10^{12}$ | $1.8 \times 10^{11}$ | |
| | | $-4.4 \times 10^{12}$ | $1.1 \times 10^{11}$ | |

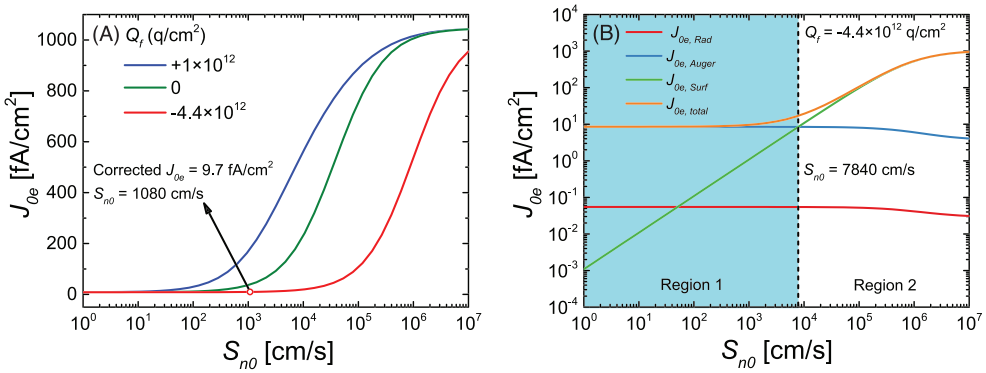


**FIGURE 8** (A) Simulated $J_{0e}$ as a function of the electron surface recombination velocity ($S_{n0}$) and the fixed charge density ($Q_f$) for symmetrically boron diffused emitter lifetime samples (emitter sheet resistance of 104 Ω/sq); (B) simulated $J_{0e}$ loss analysis by various recombination mechanisms as a function of $S_{n0}$. The lifetime samples were symmetrically passivated by tube-type PEALD $Al_2O_3$. [Colour figure can be viewed at wileyonlinelibrary.com]

2. At the boron diffused emitter, the electron surface recombination velocity ($S_{n0}$) was introduced to embody and quantify the recombination activity of the interface. $S_{n0}$ was defined as[74–76]:

$$S_{n0} = kT\sigma_n v_{th} D_{it}(E) \quad (2)$$

where $k$ is the Boltzmann constant, $T$ is the temperature in Kelvin, $\sigma_n$ is the electron capture coefficient, and $v_{th}$ is the carrier mean thermal velocity, $D_{it}(E)$ is the interface defect distribution. Hence, the electron capture coefficient $\sigma_n$ can be extracted when $S_{n0}$ was fitted to match the measured $J_{0e}$ of the sample. The simulated $J_{0e}$ as a function of $S_{n0}$ and the simulated $J_{0e}$ loss analysis by various recombination mechanisms as a function of $S_{n0}$ are shown in Figure 8A and Figure 8B, respectively.

As shown in Figure 8A, $Q_f$ has a strong impact on the boron emitter passivation. A high negative $Q_f$ is beneficial for achieving good boron emitter passivation. To further understand the underlying mechanism, $J_{0e}$ loss analysis with the contributing recombination mechanisms as a function of $S_{n0}$ was carried out and the results are shown in Figure 8B. As can be seen from Figure 8B, the contribution from radiative recombination ($J_{0e,Rad}$) is very small and negligible. As previously mentioned, SRH recombination in the emitter was not taken into account in this work. The total $J_{0e}$ ($J_{0e,total}$) was mainly dominated by the Auger recombination ($J_{0e,Auger}$) and surface recombination by the SRH recombination ($J_{0e,Surf}$). A crossover point can be seen where $J_{0e,Auger}$ and $J_{0e,Surf}$ are equal which is at an $S_{n0}$ value of around 7840 cm/s. For $S_{n0}$ values below 7840 cm/s (Region 1), $J_{0e}$ is dominated by Auger recombination and is not very sensitive to changes in $S_{n0}$. For $S_{n0}$ values above 7840 cm/s (Region 2), surface recombination becomes the primary limiting loss mechanism of $J_{0e}$. The slight reduction in Auger, radiative, and SRH recombination for very high $S_{n0}$ values is due to a reduction in the minority carrier concentration in the boron emitter due to increasingly large recombination at the surface. From Figure 8A, we can see that $J_{0e}$ saturates to a minimum value $J_{0e,min}$ of 8.6 fA/cm$^2$. In the previous part, the measured $J_{0e}$ from lifetime samples was from 15 to 19 fA/cm$^2$. Since the simulations presented in Figure 8 are done in 1D, the experimental $J_{0e}$ values should be corrected for surface area using the experimentally determined area enhancement factor of ~1.5 for pyramid textured surfaces.[77,78] Hence, the corrected $J_{0e}$ is in the range of 9.7 to 13 fA/cm$^2$, and the corresponding $S_{n0}$ is in the range of 1080 to 3750 cm/s. These values are located in Region 1, which indicates that $J_{0e}$ is limited by the Auger recombination and excellent emitter surface passivation was achieved by the developed tube-type PEALD $Al_2O_3$. To verify the accuracy of the simulation, the $\sigma_n$ was calculated based on Equation (2) and the measured energy-dependent $D_{it}(E)$. The corresponding value of (2–9) × $10^{-15}$ cm$^2$ is consistent with the $\sigma_n$ range reported for the Si/$Al_2O_3$ interface by Werner et al.[79] and Saint-Cast et al.[80]

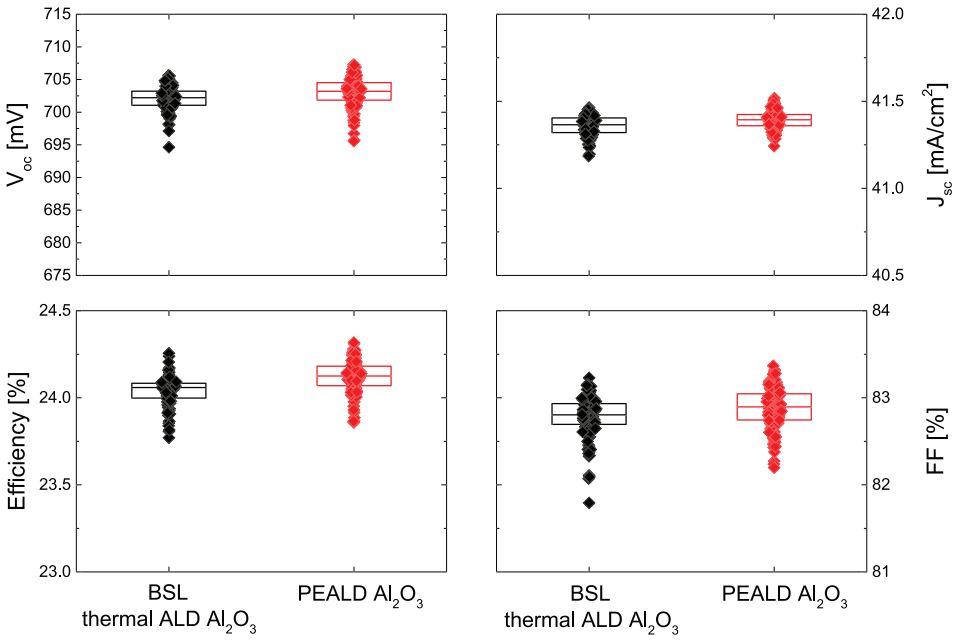


**FIGURE 9** Cell performance metrics of TOPCon samples with the newly developed industrial tube-type PEALD $Al_2O_3$ [Colour figure can be viewed at wileyonlinelibrary.com]

**TABLE 2** Summary of the *I-V* results, based on the batch average value (100–150 cells)

| | Efficiency (%) | $V_{oc}$ (mV) | $J_{sc}$ (fA/cm$^2$) | FF (%) |
|---|---|---|---|---|
| BSL (thermal ALD $Al_2O_3$) | 24.04 | 702 | 41.36 | 82.8 |
| PEALD $Al_2O_3$ | 24.1 | 703 | 41.39 | 82.9 |
| Best cell | 24.3 | 707 | 41.41 | 83.1 |
| Certified cell | 24 | 709 | 40.1 | 84.4 |

### 3.4 | Solar cell performance

To verify the performance of the newly developed industrial tube-type PEALD $Al_2O_3$ passivation at the device level, TOPCon cells were fabricated based on the industrial process flow shown in Figure 2. The measured *I-V* parameters are shown in Figure 9 and the batch average values are summarized in Table 2. An average cell efficiency of 24.1% was achieved with a $V_{oc}$ of 703 mV. The average $V_{oc}$ was 1 mV higher than the baseline group with the state-of-the-art thermal ALD $Al_2O_3$. For the best cell, a $V_{oc}$ up to 707 mV was achieved. A certified cell result of 24% by the National Institute of Metrology China is also included Table 2, with a bifacility >85%. The lower current and higher fill factor for the calibrated cell likely resulted from a difference in contacting and reflection of the measurement chuck between the two measurements. This indicates that the developed industrial tube-type PEALD $Al_2O_3$ and PECVD $SiN_x$ stack passivated the textured boron emitter effectively at the device level. This could greatly help reduce the manufacturing cost for TOPCon solar cells and foster its commercialization.

## 4 | CONCLUSION

In conclusion, we demonstrated that the champion lab-scale surface passivation can now be achieved in a new tube-type industrial PEALD reactor. State-of-the-art results were obtained on industrial textured boron emitter with a sheet resistance of 104 Ω/sq with $J_{0e}$ values down to 15 fA/cm$^2$ and $iV_{oc}$ values up to 721 mV. The results improve upon earlier results for textured boron emitters passivated by thermal $SiO_2$, ALD $TiO_2$, ALD $Al_2O_3$/PECVD $SiN_x$ stack, PECVD $AlO_x/SiN_x$ stack, and PECVD $SiO_x/SiN_x$ stack. The tube-type PEALD $Al_2O_3$ films had a $D_{it}$ of $1.1 \times 10^{11}$ cm$^{-2}$ eV$^{-1}$ and $Q_f$ of $-4.5 \times 10^{12}$ q/cm$^2$ on undiffused *c*-Si, indicating an excellent chemical passivation and field-effect passivation comparable with the state-of-the-art laboratory results by the remote plasma PEALD technology. Simulation results showed that the obtained $J_{0e}$ was quite close to its intrinsic limit, where the $J_{0e}$ was solely ruled by Auger recombination. Lastly, the tube-type PEALD $Al_2O_3$ films were applied to industrial TOPCon solar cells where an average cell efficiency above 24% with a maximum $V_{oc}$ of 707 mV was obtained. This work opens a new route for mass production of high-efficiency industrial TOPCon solar cells that are not limited by recombination at $Al_2O_3$ passivated highly doped boron emitter surface with a lean and cost-effective method. This tube-type PEALD process can easily be integrated in tube-based PECVD systems and therefore significantly simplifies the manufacturing complexity and reduces cost for commercial TOPCon solar cells.

### ACKNOWLEDGEMENTS

The authors acknowledge the support from the industrial partners, namely, Leadmicro Nano-Equipment Technology Ltd., Jinko Solar

Holding Co., Ltd., Tongwei Solar Co., Ltd., and Jolywood Solar Technology Co. Ltd. This research is supported by the Research Funding for High-level Talents of Nantong University (No. 03083035); the Major Program for the Natural Science Research of the Higher Education Institutions of Jiangsu Province, China (No. 19KJ320004); the Construction Fund for School of Tongke Microelectronics, Nantong University (No. 0702610104); and the Major State Basic Research Development Program of China (2018YFB1500501). X. Wu acknowledges the support from the Australian Government Research Training Program (RTP) Scholarship. B. Liao acknowledges the support of the "Distinguished Professor of Jiangsu Province" award.

## DATA AVAILABILITY STATEMENT

The data that support the findings of this study are available from the corresponding author upon reasonable request.

## ORCID

*Baochen Liao* https://orcid.org/0000-0003-2860-8942
*Xinyuan Wu* https://orcid.org/0000-0002-7908-3296
*Shaozhou Wang* https://orcid.org/0000-0002-7299-3481

## REFERENCES

1. Blakers AW, Wang A, Milne AM, Zhao J, Green MA. 22.8% efficient silicon solar cell. *Appl Phys Lett*. 1989;55(13):1363-1365. doi:10.1063/1.101596
2. Zhao J, Wang A, Green MA. 24·5% efficiency silicon PERT cells on MCZ substrates and 24·7% efficiency PERL cells on FZ substrates. *Prog Photovolt*. 1999;7(6):471-474. doi:10.1002/(SICI)1099-159X(199911/12)7:63.0.CO;2-7
3. Chen R, Tong H, Zhu H, et al. 23.83% efficient mono-PERC incorporating advanced hydrogenation. *Prog Photovolt*. 2020;28(12):1239-1247. doi:10.1002/pip.3243
4. Min B, Muller M, Wagner H, et al. A roadmap toward 24% efficient PERC solar cells in industrial mass production. *IEEE J Photovolt*. 2017;7(6):1541-1550. doi:10.1109/JPHOTOV.2017.2749007
5. Schmidt J, Peibst R, Brendel R. Surface passivation of crystalline silicon solar cells: present and future. *Sol Energy Mater Sol Cells*. 2018;187:39-54. doi:10.1016/j.solmat.2018.06.047
6. Saint-Cast P, Werner S, Greulich J, et al. Analysis of the losses of industrial-type PERC solar cells. *Phys Status Solidi A*. 2017;214(3):1600708. doi:10.1002/pssa.201600708
7. Huang H, Lv J, Bao Y, et al. 20.8% industrial PERC solar cell: ALD Al2O3 rear surface passivation, efficiency loss mechanisms analysis and roadmap to 24%. *Sol Energy Mater Sol Cells*. 2017;161:14-30. doi:10.1016/j.solmat.2016.11.018
8. Müller M, Fischer G, Bitnar B, et al. Loss analysis of 22% efficient industrial PERC solar cells. *Energy Procedia*. 2017;124:131-137. doi:10.1016/j.egypro.2017.09.322
9. Altermatt PP Yang Y, Chen Y, Chen D, Zhang X, Xu G, Feng Z. Learning from the past to look beyond the roadmap of PERC Si solar cell mass production. In 35th European photovoltaic solar energy conference and exhibition. Brussels, Belgium; 2018:215–221.
10. Feldmann F, Simon M, Bivour M, Reichel C, Hermle M, Glunz SW. Carrier-selective contacts for Si solar cells. *Appl Phys Lett*. 2014;104:181105. doi:10.1063/1.4875904
11. Melskens J, van de Loo BWH, Macco B, Black LE, Smit S, Kessels WMM. Passivating contacts for crystalline silicon solar cells: from concepts and materials to prospects. *IEEE J Photovolt*. 2018;8(2):373-388. doi:10.1109/JPHOTOV.2018.2797106
12. Allen TG, Bullock J, Yang X, Javey A, De Wolf S. Passivating contacts for crystalline silicon solar cells. *Nat Energy*. 2019;4(11):914-928. doi:10.1038/s41560-019-0463-6
13. Tanaka M, Taguchi M, Takahama T, et al. development of a new heterojunction structure (ACJ-HIT) and its application to polycrystalline silicon solar cells. *Prog Photovolt*. 1993;1(2):85-92. doi:10.1002/pip.4670010201
14. Taguchi M, Kawamoto K, Tsuge S, et al. HITTM cells—high-efficiency crystalline Si cells with novel structure. *Prog Photovolt*. 2000;8(5):503-513. doi:10.1002/1099-159X(200009/10)8:53.0.CO;2-G
15. Tsunomura Y, Yoshimine Y, Taguchi M, et al. Twenty-two percent efficiency HIT solar cell. *Sol Energy Mater Sol Cells*. 2009;93(6–7):670-673. doi:10.1016/j.solmat.2008.02.037
16. Taguchi M, Yano A, Tohoda S, et al. 24.7% record efficiency HIT solar cell on thin silicon wafer. *IEEE J Photovolt*. 2013;4(1):96-99. doi:10.1109/JPHOTOV.2013.2282737
17. Adachi D, Hernández JL, Yamamoto K. Impact of carrier recombination on fill factor for large area heterojunction crystalline silicon solar cell with 25.1% efficiency. *Appl Phys Lett*. 2015;107:233506. doi:10.1063/1.4937224
18. Yoshikawa K, Yoshida W, Irie T, et al. Exceeding conversion efficiency of 26% by heterojunction interdigitated back contact solar cell with thin film Si technology. *Sol Energy Mater Sol Cells*. 2017;173:37-42. doi:10.1016/j.solmat.2017.06.024
19. Yoshikawa K, Kawasaki H, Yoshida W, et al. Silicon heterojunction solar cell with interdigitated back contacts for a photoconversion efficiency over 26%. *Nat Energy*. 2017;2(5):17032. doi:10.1038/nenergy.2017.32
20. Masuko K, Shigematsu M, Hashiguchi T, et al. Achievement of more than 25% conversion efficiency with crystalline silicon heterojunction solar cell. *IEEE J Photovolt*. 2014;4(6):1433-1435. doi:10.1109/JPHOTOV.2014.2352151
21. Carroll D. Australian startup sets 25.54% efficiency record for silicon cell. 2021. Available: https://www.pv-magazine.com/2021/09/10/australian-startup-sets-25-54-efficiency-record-for-silicon-cell/
22. Feldmann F, Bivour M, Reichel C, Hermle M, Glunz SW. Passivated rear contacts for high-efficiency n-type Si solar cells providing high interface passivation quality and excellent transport characteristics. *Sol Energy Mater Sol Cells*. 2014;120:270-274. doi:10.1016/j.solmat.2013.09.017
23. Feldmann F, Bivour M, Reichel C, Steinkemper H, Hermle M, Glunz SW. Tunnel oxide passivated contacts as an alternative to partial rear contacts. *Sol Energy Mater Sol Cells*. 2014;131:46-50. doi:10.1016/j.solmat.2014.06.015
24. Römer U, Peibst R, Ohrdes T, et al. Recombination behavior and contact resistance of n+ and p+ poly-crystalline Si/mono-crystalline Si junctions. *Sol Energy Mater Sol Cells*. 2014;131:85-91. doi:10.1016/j.solmat.2014.06.003
25. Richter A, Benick J, Feldmann F, Fell A, Hermle M, Glunz SW. N-type Si solar cells with passivating electron contact: identifying sources for efficiency limitations by wafer thickness and resistivity variation. *Sol Energy Mater Sol Cells*. 2017;173:96-105. doi:10.1016/j.solmat.2017.05.042
26. Yan D, Phang SP, Wan Y, Samundsett C, Macdonald D, Cuevas A. High efficiency n-type silicon solar cells with passivating contacts based on PECVD silicon films doped by phosphorus diffusion. *Sol Energy Mater Sol Cells*. 2019;193:80-84. doi:10.1016/j.solmat.2019.01.005
27. Chen D, Chen Y, Wang Z, et al. 24.58% total area efficiency of screen-printed, large area industrial silicon solar cells with the tunnel oxide passivated contacts (i-TOPCon) design. *Sol Energy Mater Sol Cells*. 2020;206:110258. doi:10.1016/j.solmat.2019.110258
28. Chen W et al. Influence of PECVD deposition temperature on phosphorus doped poly-silicon passivating contacts. *Sol Energy Mater Sol Cells*. 2020;206:110348.

29. Nandakumar N, Rodriguez J, Kluge T, et al. approaching 23% with large-area monoPoly cells using screen-printed and fired rear passivating contacts fabricated by inline PECVD. *Prog Photovolt*. 2018;27:107-112. doi:10.1002/pip.3097
30. Gao T et al. An industrially viable TOPCon structure with both ultrathin SiOx and n+−poly-Si processed by PECVD for p-type c-Si solar cells. *Sol Energy Mater Sol Cells*. 2019;200:109926.
31. Yan D, Cuevas A, Michel JI, et al. Polysilicon passivated junctions: the next technology for silicon solar cells? *Joule*. 2021;5(4):811-828. doi:10.1016/j.joule.2021.02.013
32. Richter A et al. Design rules for high-efficiency both-sides-contacted silicon solar cells with balanced charge carrier transport and recombination losses. *Nat Energy*. 2021;6:429-438.
33. Haase F, Hollemann C, Schäfer S, et al. Laser contact openings for local poly-Si-metal contacts enabling 26.1%-efficient POLO-IBC solar cells. *Sol Energy Mater Sol Cells*. 2018;186:184-193. doi:10.1016/j.solmat.2018.06.020
34. Singha B, Solanki CS. N-type solar cells: advantages, issues, and current scenarios. *Mater Res Express*. 2017;4(7):072001. doi:10.1088/2053-1591/aa6402
35. Chen D et al. Hydrogen-induced degradation: explaining the mechanism behind light-and elevated temperature-induced degradation in n-and p-type silicon. *Sol Energy Mater Sol Cells*. 2020;207:110353.
36. Chen D, Contreras MV, Ciesla A, et al. Progress in the understanding of light- and elevated temperature-induced degradation in silicon solar cells: a review. *Prog Photovolt*. 2020;29:1180-1201.
37. Zhang Z, Liao M, Huang Y, et al. Improvement of surface passivation of tunnel oxide passivated contact structure by thermal annealing in mixture of water vapor and nitrogen environment. *Solar RRL*. 2019;3:1900105.
38. Liao B, Stangl R, Ma F, et al. Deposition temperature independent excellent passivation of highly boron doped silicon emitters by thermal atomic layer deposited Al2O3. *J Appl Phys*. 2013;114(9):094505. doi:10.1063/1.4819970
39. Liao B, Stangl R, Ma F, et al. Excellent c-Si surface passivation by thermal atomic layer deposited aluminum oxide after industrial firing activation. *J Phys D Appl Phys*. 2013;46:385102.
40. Hoex B, Heil S, Langereis E, Van de Sanden M, Kessels W. Ultralow surface recombination of c-Si substrates passivated by plasma-assisted atomic layer deposited $Al_2O_3$. *Appl Phys Lett*. 2006;89:042112.
41. Hoex B, Schmidt J, Bock R, Altermatt P, Van De Sanden M, Kessels W. Excellent passivation of highly doped p-type Si surfaces by the negative-charge-dielectric $Al_2O_3$. *Appl Phys Lett*. 2007;91:112107. doi:10.1063/1.2784168
42. Hoex B, Schmidt J, Pohl P, Van de Sanden M, Kessels W. Silicon surface passivation by atomic layer deposited $Al_2O_3$. *J Appl Phys*. 2008;104:044903.
43. Dingemans G, Terlinden NM, Pierreux D, Profijt HB, van de Sanden MCM, Kessels WMM. Influence of the oxidant on the chemical and field-effect passivation of Si by ALD $Al_2O_3$. *Electrochem Solid St*. 2011;14(1):H1. doi:10.1149/1.3501970
44. Johnson RW, Hultqvist A, Bent SF. A brief review of atomic layer deposition: from fundamentals to applications. *Mater Today*. 2014;17:236-246.
45. George SM. Atomic layer deposition: an overview. *Chem Rev*. 2010;110:111-131.
46. Sinton RA, Cuevas A. Contactless determination of current–voltage characteristics and minority-carrier lifetimes in semiconductors from quasi-steady-state photoconductance data. *Appl Phys Lett*. 1996;69(17):2510-2512. doi:10.1063/1.117723
47. Kane DE, Swanson RM. Measurement of the emitter saturation current by a contactless photoconductivity decay method. In 18th IEEE PVSC, Las Vegas, USA; 1985: 578–583.
48. Sinton RA, Swanson RM. Recombination in highly injected silicon. *IEEE Trans Electron Devices*. 1987;34(6):1380-1389. doi:10.1109/T-ED.1987.23095
49. Sproul AB, Green MA. Improved value for the silicon intrinsic carrier concentration from 275 to 375 K. *J Appl Phys*. 1991;70(2):846-854. doi:10.1063/1.349645
50. Liao B, Stangl R, Ma F, et al. Deposition temperature independent excellent passivation of highly boron doped silicon emitters by thermal atomic layer deposited Al2O3. *J Appl Phys*. 2013;114:094505.
51. Thomson AF, Hameiri Z, Grant NE, Price CJ, Di Y, Spurgin J. Uncertainty in photoconductance measurements of the emitter saturation current. *IEEE J Photovolt*. 2013;3(4):1200-1207. doi:10.1109/JPHOTOV.2013.2270346
52. Wilson M, Lagowski J, Jastrzebski L, Savtchouk A, Faifer V. COCOS (corona oxide characterization of semiconductor) non-contact metrology for gate dielectrics. In NIST Conference on Characterization and Metrology for ULSI Technology, Maryland, USA. 2001;550:220–225.
53. Wilson M, Marinskiy D, Byelyayev A, et al. The present status and recent advancements in corona-kelvin non-contact electrical metrology of dielectrics for IC-manufacturing. *ECS Trans*. 2006;3(3):3-24. doi:10.1149/1.2355694
54. Wilson M, D'amico J, Savtchouk A, Edelman P, Findlay A, Jastrzebski L, Lagowski J, Kis-Szabo K, Korsos F, Toth A, Pap A. Multifunction metrology platform for photovoltaics. In 37th IEEE conference, Washington DC, USA; 2011:1748–1753.
55. McIntosh KR, Altermatt PP. A freeware 1D emitter model for silicon solar cells. In The 35th IEEE PVSC, Honolulu, USA; 2010:2188–2193.
56. Klaassen DBM. A unified mobility model for device simulation-I. model equations and concentration dependence. *Solid-State Electron*. 1992;35(7):953-959. doi:10.1016/0038-1101(92)90325-7
57. Klaassen DBM. A unified mobility model for device simulation-II. Temperature dependence of carrier mobility and lifetime. *Solid-State Electron*. 1992;35(7):961-967. doi:10.1016/0038-1101(92)90326-8
58. Pässler R. Dispersion-related description of temperature dependencies of band gaps in semiconductors. *Physical Rev B*. 2002;66(8):085201. doi:10.1103/PhysRevB.66.085201
59. Altermatt PP, Schenk A, Heiser G. A simulation model for the density of states and for incomplete ionization in crystalline silicon. I. Establishing the model in Si:P. *J Appl Phys*. 2006;100(11):113714. doi:10.1063/1.2386934
60. Dirac PAM. On the theory of quantum mechanics. *Proc Royal Soc A*. 1926;112(762):661-677. doi:10.1098/rspa.1926.0133
61. Altermatt PP, Schumacher JO, Cuevas A, et al. Numerical modeling of highly doped Si:P emitters based on Fermi–Dirac statistics and self-consistent material parameters. *J Appl Phys*. 2002;92(6):3187-3197. doi:10.1063/1.1501743
62. Schenk A. Finite-temperature full random-phase approximation model of band gap narrowing for silicon device simulation. *J Appl Phys*. 1998;84(7):3684-3695. doi:10.1063/1.368545
63. Altermatt PP, Schenk A, Geelhaar F, Heiser G. Reassessment of the intrinsic carrier density in crystalline silicon in view of band-gap narrowing. *J Appl Phys*. 2003;93(3):1598-1604. doi:10.1063/1.1529297
64. Trupke T, Green MA, Würfel P, et al. Temperature dependence of the radiative recombination coefficient of intrinsic crystalline silicon. *J Appl Phys*. 2003;94(8):4930. doi:10.1063/1.1610231
65. McIntosh KR, Black LE. On effective surface recombination parameters. *J Appl Phys*. 2014;116:014503.
66. Richter A, Glunz SW, Werner F, Schmidt J, Cuevas A. Improved quantitative description of auger recombination in crystalline silicon. *Physical Rev B*. 2012;86:165202.ator> doi:
67. Cornagliotti E, Uruena A, Aleman M, et al. Large-area n-type PERT solar cells featuring rear p+ emitter passivated by ALD Al2 O3. *IEEE J Photovolt*. 2015;5(5):1366-1372. doi:10.1109/JPHOTOV.2015.2458041

68. Liao B, Hoex B, Shetty KD, Basu PK, Bhatia CS. Passivation of boron-doped industrial silicon emitters by thermal atomic layer deposited titanium oxide. *IEEE J Photovolt*. 2015;5(4):1062-1066. doi:10.1109/JPHOTOV.2015.2434596
69. Fernandez-Robledo S, Kluska S, Greulich J, Nekarda J. Selective boron emitters using laser-induced forward transfer versus laser doping from borosilicate glass. *IEEE J Photovolt*. 2017;7(5):1254-1263. doi:10.1109/JPHOTOV.2017.2717338
70. Duttagupta S, Lin F, Shetty KD, Aberle AG, Hoex B. Excellent boron emitter passivation for high-efficiency Si wafer solar cells using $AlO_x/SiN_x$ dielectric stacks deposited in an industrial inline plasma reactor. *Prog Photovolt*. 2013;21:760-764. doi:10.1002/pip.1259
71. Duttagupta S, Ma F-J, Hoex B, Aberle AG. Excellent surface passivation of heavily doped p+ silicon by low-temperature plasma-deposited $SiO_x/SiN_y$ dielectric stacks with optimised antireflective performance for solar cell application. *Sol Energy Mater Sol Cells*. 2014;120:204-208. doi:10.1016/j.solmat.2013.09.004
72. Richter A, Benick J, Hermle M, Glunz SW. Excellent silicon surface passivation with 5 Å thin ALD $Al_2O_3$ layers: influence of different thermal post-deposition treatments. *Phys Status Solidi RRL*. 2011;5(5-6):202-204. doi:10.1002/pssr.201105188
73. Richter A, Benick J, Hermle M. Boron emitter passivation with $Al_2O_3$ and $Al_2O_3/SiN_x$ stacks using ALD $Al_2O_3$. *IEEE J Photovolt*. 2013;3(1):236-245. doi:10.1109/JPHOTOV.2012.2226145
74. Girisch RBM, Mertens RP, De Keersmaecker RF. Determination of Si-SiO/sub 2/interface recombination parameters using a gate-controlled point-junction diode under illumination. *IEEE Trans Electron Devices*. 1988;35:203-222.
75. Shockley W, Read W Jr. Statistics of the recombinations of holes and electrons. *Phys Rev*. 1952;87(5):835-842. doi:10.1103/PhysRev.87.835
76. Aberle AG, Glunz S, Warta W. Impact of illumination level and oxide parameters on Shockley–Read–hall recombination at the $Si-SiO_2$ interface. *J Appl Phys*. 1992;71:4422-4431.
77. Baker-Finch SC, McIntosh KR. The contribution of planes, vertices, and edges to recombination at pyramidally textured surfaces. *IEEE J Photovolt*. 2011;1(1):59-65. doi:10.1109/JPHOTOV.2011.2165530
78. Baker-Finch SC, Mcintosh KR. Reflection distributions of textured monocrystalline silicon: implications for silicon solar cells. *Prog Photovolt*. 2012;960-971. doi:10.1002/pip.2186
79. Werner F, Cosceev A, Schmidt J. Silicon surface passivation by $Al_2O_3$: recombination parameters and inversion layer solar cells. *Energy Procedia*. 2012;27:319-324. doi:10.1016/j.egypro.2012.07.070
80. Saint-Cast P, Heo YH, Billot E, et al. Variation of the layer thickness to study the electrical property of PECVD $Al_2O_3$/c-Si interface. *Energy Procedia*. 2011;8:642-647. doi:10.1016/j.egypro.2011.06.195


**How to cite this article:** Liao B, Wu X, Wu W, et al. Tube-type plasma-enhanced atomic layer deposition of aluminum oxide: Enabling record lab performance for the industry with demonstrated cell efficiencies >24%. *Prog Photovolt Res Appl*. 2022;1-10. doi:10.1002/pip.3607